

Catalyst-Trap Microreactor for Hydrogenation of a Pharmaceutical Intermediate

S. McGovern¹, H. Gadre¹, R.S. Besser¹, C.S. Pa², W. Mansfield², S. Pau²

¹Chemical, BioMedical, & Materials Engineering Department, Stevens Institute of Technology, Castle Point on Hudson, Hoboken, NJ 07030, 201.216.5257, rbesser@stevens.edu

²New Jersey Nanotechnology Consortium (NJNC) at Lucent-Bell Labs, 600 Mountain Avenue, Murray Hill, NJ 07974

Abstract

A silicon microreactor has been developed to investigate gas-liquid-solid catalytic reactions. The reactor employs a three-channel “catalyst-trap” design, whereby solid catalyst is suspended in the liquid channel by an arrangement of posts. Such a device has advantages in that commercial catalysts are supported, and that pressure drop across the bed can be reduced by engineering the packing density. A model incorporating the transport and kinetic effects is developed to design the reactor. The reaction chosen is one in a family of reactions relevant to the pharmaceutical industry, the liquid-phase hydrogenation of o-nitroanisole to o-anisidine. The reaction is carried out across a range of gas and liquid flow rates that encompasses three distinct flow regimes, termed gas-dominated, liquid-dominated, and transitional. Experiments seek to assign a reaction conversion and selectivity to each point in this two-phase “flow map”, then reconcile differences in performance with the characteristics of the respective flow regime. We observe the highest reaction conversion in the transitional flow regime, where competition between the two phases results in the generation of a large amount of gas-liquid interfacial area. The experimental conversion is greater than that predicted by the model, an effect attributable to the mass transfer enhancement induced by transitional flow. Reaction time within the microchannel is sufficiently small so that selectivity towards production of o-anisidine is nearly 100% across all flow regimes. In this work we relate our map of conversion to the flow behavior and reactor geometry, and we discuss steps for further exploring the mass transfer characteristics of the transitional flow regime. This reactor architecture may be useful for catalyst evaluation through rapid screening, or in large numbers as an alternative to macro-scale production reactors.

Introduction

The term “microreactor” is broadly used to describe devices ranging from tens of microns to several centimeters in size. Microreactor technology possesses significant advantages over conventional macro-scale reactors. Because of their small size, microreactors have inherently large surface-to-volume ratios, allowing for superior mass and heat transport. Surface-to-volume ratios of 20,000 m²/m³ or more are not uncommon, compared to 1,000 m²/m³ for a conventional reactor. In the case of catalytic reactions, where competition exists between the rate of diffusion to the catalyst sites and the rate of reaction, microreactors are able to virtually eliminate mass transport resistance, making them an extremely useful tool for isolating reaction kinetics. Excellent heat transfer properties ensure a uniform temperature throughout the reactor and prevent the formation of hotspots in the case of an exothermic reaction. In a stirred-tank reactor, for example, hotspots can lead to undesired changes in local concentration or pH. Low residence time and ease of heat removal also make microreactors more suitable for flammable service, where the potential for explosion or fire is greatly reduced.

In this paper, we consider the use of a microreactor for gas-liquid-solid catalytic reactions, where the rate of diffusion of gas into the liquid phase can also limit the observed reaction rate. Thus, we would like to be able to address both intra-particle and inter-particle diffusion. The former can be accomplished with reasonable certainty simply by using small-sized catalyst particles. In general, catalyst particles with a diameter smaller than $100\ \mu\text{m}$ ($1 \times 10^{-4}\ \text{m}$) exhibit sufficiently low transport resistance to enable their use with most reactions [9]. The latter is a function of gas-liquid interfacial area and driving force for transport, both of which depend on the gas-liquid flow regime.

For our purposes, three traditional flow regimes are adequate to describe the two-phase behavior, although other papers present more precise delineations [7]. Bubble flow is characterized by liquid as the continuous phase, with bubbles of gas dispersed into a fully-wetted channel. As the ratio of gas-to-liquid velocity increases, the Taylor (slug) flow regime emerges, in which alternating segments of gas and liquid occupy the channel. The relative lengths of each segment are constant for a given set of inlet conditions. As gas-to-liquid velocity further increases, annular (for a capillary) or trickle (for a wide reaction channel) flow occurs. In annular or trickle flow, gas is the continuous phase, and the liquid flows as a thin film along the channel walls [7]. Figure 1 illustrates the three flow regimes, where u_G and u_L are the gas and liquid superficial velocities, respectively.

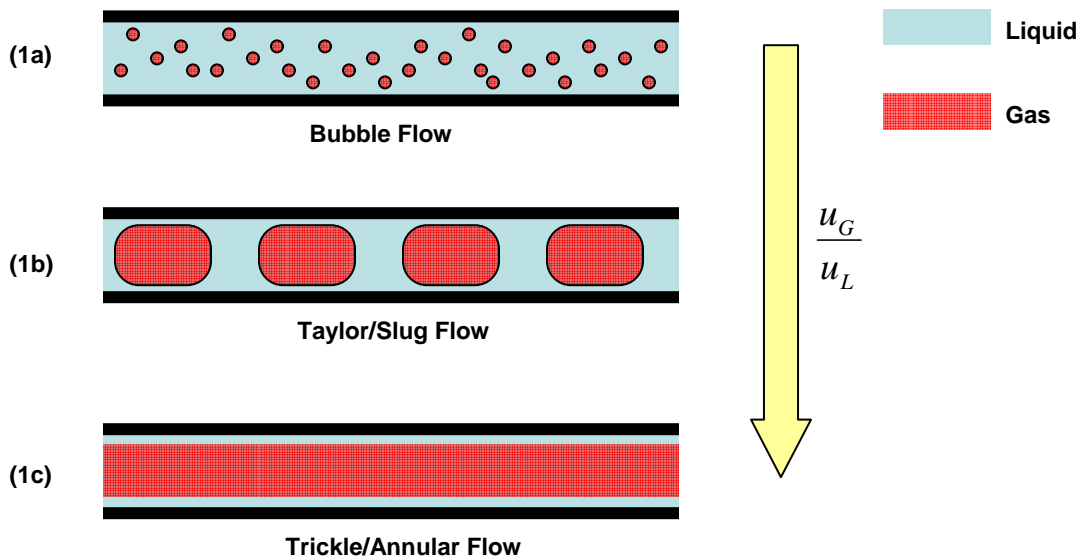


Figure 1- Illustration of Gas/Liquid Flow Regimes

In the context of a gas-liquid-solid catalytic reaction with reaction occurring in the liquid phase, two characteristics are critical in evaluating the advantages and disadvantages of a particular flow regime. First, we desire good mass transport between gas and liquid, which depends on the driving force for mass transport and the gas-liquid interfacial area created. Second, we desire a high liquid-solid interfacial area to effectively utilize the catalyst for rate of production. The highest liquid-solid interfacial area will be achieved when liquid is the continuous phase.

The slug flow regime in a capillary is typically associated with the best gas-liquid mass transport because of the no-slip condition at the channel walls. The high velocity gradient within the liquid slug provides turbulence, so a constant refreshing of the gas-liquid interface occurs. This provides a high driving force for diffusion at the interface, and good mixing within the liquid. Despite good mass transport properties, slug flow does not maximize the liquid-solid interfacial area because gas still occupies a significant portion of the channel. Bubble flow, in contrast, exhibits both a high liquid-solid and gas-liquid interfacial area. Because liquid is the continuous phase with only small pockets of gas, essentially all of the catalyst is in contact with liquid [6]. Thus we can generalize that slug flow will possess the best gas-liquid mass transport, owing to both interfacial area and driving force, and that bubble flow, although less turbulent, will have the highest liquid-solid interfacial area. On the basis of these mass transfer arguments, we speculate that the best reactor performance will fall in either the bubble or slug flow regimes. Likewise, we suppose that trickle flow, with the lowest liquid-solid and gas-liquid interfacial areas, will be the least effective for this particular reaction. We proceed to design the device and subsequent experiments with this hypothesis in mind.

Reactor Modeling, Design, and Fabrication

The reactor is designed for operation across the spectrum of flow regimes, while making use of the advantages of microchemical systems to relieve various transport resistances. The design is pictured below in Figure 2.

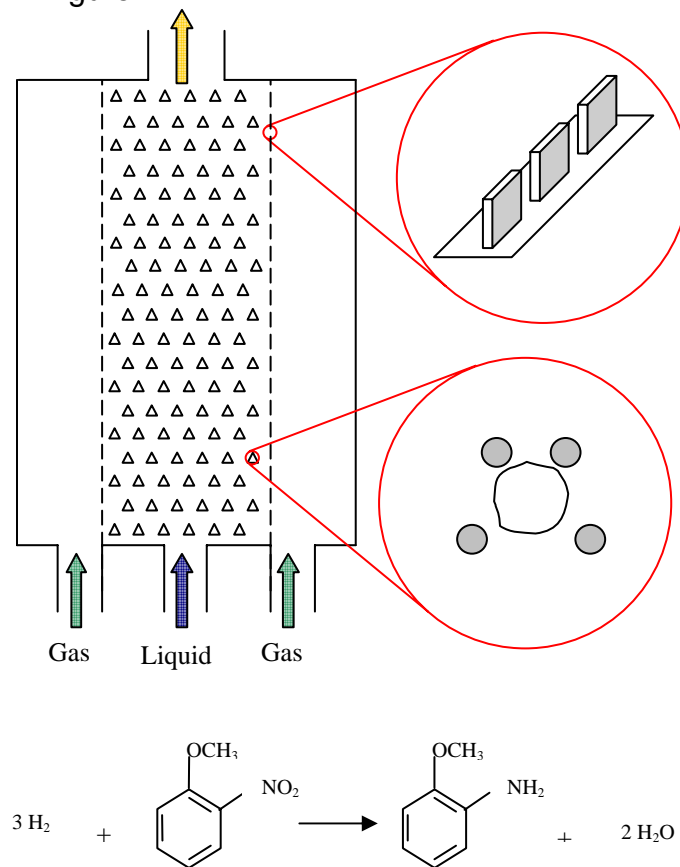


Figure 2- Proposed Reactor Design

The reactor will be used for the liquid-phase hydrogenation of o-nitroanisole to o-anisidine, with methanol as an inert solvent. The catalyst is 5% Pd by weight on carbon. Hydrogen gas enters along the two outside channels, and is allowed to diffuse into the liquid channel through a slotted wall, shown at the top inset. The reaction occurs in the liquid channel, where an arrangement of posts, or catalyst traps, holds the catalyst particles in place (lower inset). Each trap is a trapezoidal arrangement of four posts spanning the depth of the channel. The posts are spaced to “catch” catalyst particles and hold them in place, so one can imagine the liquid sees the particles stacked single-file on top of one another as it travels down the channel. The reaction is therefore a three-step process: (1) hydrogen must diffuse through the slots and dissolve in the bulk liquid; (2) the liquid must disperse to the catalyst particles and diffuse within the particles to the reaction sites; (3) reaction occurs at the catalyst sites.

To design the reactor, we model the bulk liquid-phase concentration of all species throughout the reactor. The liquid channel is treated as a plug flow reactor with a continuous source of hydrogen available at any axial position. The slots can be sufficiently sized to allow the gas to overcome liquid surface tension and pass into the liquid channel. Hydrogen concentration in the liquid phase is therefore limited by diffusion across the gas-liquid interface. The rate of change of hydrogen concentration has two contributing terms:

$$\frac{dc_A}{dt} = [\text{Rate of diffusion from gas into liquid}] + [\text{Rate of reaction}]$$

$$\frac{dc_A}{dz} = \frac{\varepsilon}{u_L} \cdot \left[k_L \left(\frac{P_A}{H_A} - c_A \right) a_h - \frac{3w_c k c_A c_B}{(1 + K_A c_A)(1 + K_B c_B)} \right] \quad (1)$$

For the first term, the concentration of hydrogen at the gas-liquid interface is calculated from the Henry’s Law constant, H_A , for hydrogen in solutions of nitroanisole and methanol [2]. The difference between the interfacial and bulk liquid concentrations represents the driving force for diffusion. The parameter a_h is the gas-liquid interfacial area per unit volume, and is estimated from packed tower literature (strippers/absorbers) [10]. Uncertainty may exist in the application of these macroscale correlations to the microreactor geometry, but in the absence of alternatives we will use them for design purposes. The second term is the reaction rate expression [1]. For each remaining species, equation (1) will contain only the reaction term with the respective stoichiometric coefficient. The four expressions for rate of change of concentration are integrated numerically over the channel length from 0 to z . Figure 3 below shows the final liquid channel dimensions.

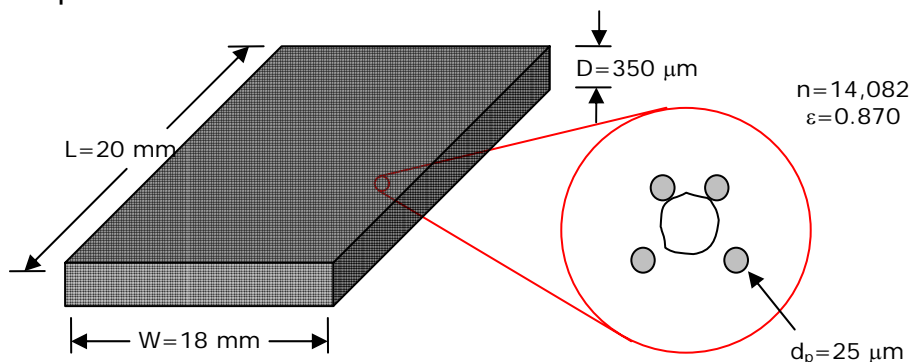


Figure 3- Design Parameters for Liquid Channel

The above dimensions are chosen to give an appreciable conversion across our target range of experimental conditions. The channel contains approximately 14,000 catalyst traps that, when loaded, give a void fraction of 0.870. The posts are 25 μm in diameter and are arranged as a trapezoid to hold a 40-50 μm particle. Traps are spaced 75 μm apart (closest edge-to-edge distance) to allow catalyst to pass through during loading.

The reactors are fabricated at NJNC-Bell Labs in Murray Hill, NJ using standard silicon photolithography techniques. Inlet and outlet ports are etched on the underside of the reactors. After etching, the silicon wafer is diced into individual chips. In our case, we received sixteen chips of dimensions 31 x 28 mm (0.031 x 0.028 m) per wafer. The reactors are then sealed by anodically bonding a piece of Pyrex glass over the surface of the chip. Anodic bonding applies voltage at high temperature, typically 1000 VDC and 450-490 C, to displace ions from the surface of the glass. The depletion of ions makes the glass surface highly reactive, forming a strong bond with the silicon substrate. The intent of the glass-covered reactor is two-fold, first as an aid in catalyst loading, and second for observation of the gas-liquid flow behavior.

Experimental

A schematic of the experimental setup is shown below in Figure 4. For overhead image and video capture, the setup includes a CCD camera above the reactor. The reactor itself is clamped onto a 4.5" x 3" stainless steel block, through which channels are machined for gas and liquid passage.

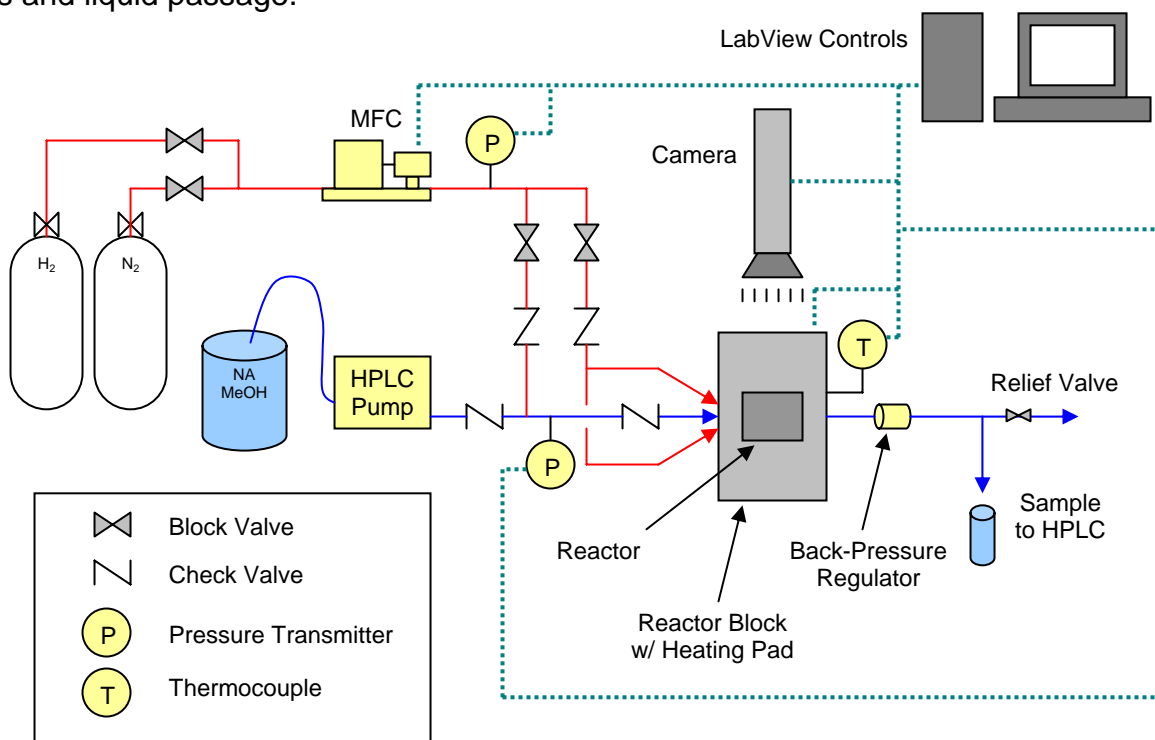


Figure 4- Schematic of Experimental Setup

We first needed a systematic assessment, or map, of the possible flow regimes as they pertained to our particular device. To construct the flow map, we used liquid flow rates ranging from 0.06 to 0.50 mL/min, and gas flow rates ranging from 2 to 20 sccm. We looked for

differences in behavior with changing conditions and approximated borders between the three flow regimes. With the flow map established, we began measuring reaction conversion and selectivity at each point on the map. Catalyst was manually loaded by inverting the reactor and applying vacuum to draw the catalyst through the inlet port. Tapping the reactor against the countertop caused the catalyst to move down the channel and settle amongst the traps. Approximately 6 mg of catalyst were used for each run. For each set of conditions, we sampled the reactor outlet periodically over the course of approximately one hour. Samples were analyzed offline in an HPLC to measure the weight fractions of o-nitroanisole and o-anisidine, from which we calculated the conversion and selectivity. After each run, we regenerated catalyst and evaporated any residual liquid by heating to 300 C for ten minutes. Reactor conditions were 30 C and 25 psia for all experiments. The feed solution was approximately 16% nitroanisole by weight.

Results and Discussion

The reactor flow map is shown below in Figure 5:

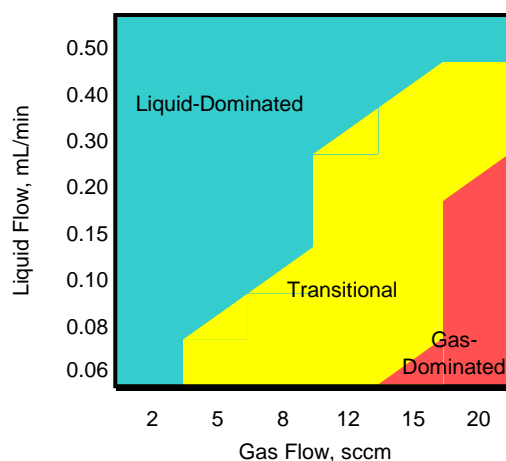


Figure 5- Reactor Flow Map

Because this particular microchannel is rectangular-shaped with a high width-to-depth ratio, it cannot be considered a capillary or cylindrical channel. Thus, the conventional nomenclature of bubble, slug, and trickle flow is not applicable to our geometry. Instead, “gas-dominated”, “liquid-dominated”, and “transitional” are more appropriate terms. Liquid- and gas-dominated flows are characterized by stable patterns in which the continuous phase impedes movement of the non-continuous phase throughout the channel. For example, in liquid-dominated flow, 80% or more of the channel volume is occupied by liquid, with several small pockets of gas. In gas-dominated flow, large gas pockets persist and force liquid to channel around them. Transitional flow is characterized by an unstable pattern in which gas and liquid compete for space within the channel. This competition causes a periodic refreshing of the gas-liquid pattern, so that in addition to significant interfacial area, high turbulence is exhibited within the channel. Pockets of gas, upon refreshing, often leave behind traps surrounded by a droplet of liquid. The small distance (~15 μm) between posts likely prevents gas from overcoming the liquid surface tension, and leaves behind “wetted” traps within the gas pocket, an effect we will discuss further when we present the reaction results. The presence of wetted traps is another indicator of transitional flow. It is important to note that the modified

terminology is intended only to help visualize the correct flow behavior, and that liquid-dominated/transitional/gas-dominated are analogous to bubble/slug/trickle in the context of the mass transfer arguments presented in the Introduction section.

We obtained the conversion results in Figure 6 for the lower third of the flow map. Each chart shows the conversion plotted against time. Error bars represent plus/minus one standard deviation for each particular set of samples.

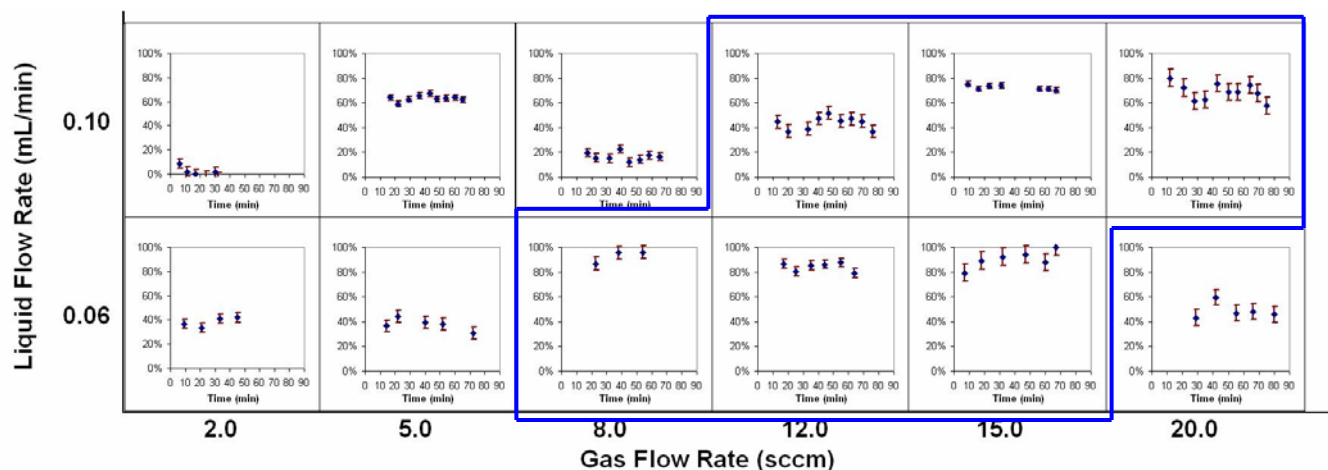


Figure 6- Conversion Results (30 C, 25 psia)

The highest conversion in Figure 6 occurs in the highlighted area, from approximately 8-15 sccm for 0.06 mL/min and 12-20 sccm for 0.10 mL/min. This range coincides with the transitional flow regime on Figure 5. Conditions outside the transitional region experienced significantly lower conversion. We also note that within a given flow regime, conversion is higher at 0.06 mL/min than at 0.10 mL/min, indicating the influence of liquid residence time, and giving some validity to the plug flow model. For all runs, the selectivity towards o-anisidine is nearly 100%, indicating that no side reactions occur. We can see from the data that over the period of approximately one hour, catalyst deactivation is negligible.

The conversion results are consistent with our premise that the best reactor performance would fall within the flow regime exhibiting either the best gas-liquid or liquid-solid mass transfer characteristics. In our case, this is transitional flow, with its continually refreshing pattern and high gas-liquid interfacial area. Though their mass transfer characteristics are similar, there is one outstanding difference between conventional slug flow and our observed transitional flow. In slug flow within a capillary, the refreshing occurs as a recirculation around the boundary of each slug. In general, slugs do not disturb the structure of adjacent slugs, and the pattern of alternating gas and liquid from one of the channel to the other is maintained. The refreshing in transitional flow affects the entire channel, as though the pattern is wiped clean and then redrawn in a different, usually random, way. Thus, it could be argued that the turbulence brought on by transitional flow enhances not only gas-liquid, but also liquid-solid mass transfer, making it clearly the preferred regime for the reaction.

The conversion predicted by the model ranges from 1.0 to 3.5% across our range of experimental conditions. The model does assume the reaction to be controlled by gas-liquid mass transfer, but even after adjusting the interfacial area parameter in equation (1), a_h , to

large values, the experimental conversion is much higher. A possible explanation is the presence of wetted versus non-wetted catalyst traps. As we discussed above, when the gas pattern refreshes it often leaves behind traps encased in droplets of liquid. One can imagine that an array of several thousand traps covered by liquid droplets approximately $100\ \mu\text{m}$ in diameter would create an extraordinary amount of gas-liquid interfacial area. If coupled with the proper refreshing gas-liquid pattern the traps would function as a network of mini-batch reactors, where refreshing periodically sweeps away the products and introduces new reactants. The droplets' small size would give very short diffusion distances for hydrogen, allowing for excellent transport of dissolved hydrogen throughout the liquid phase, and high reaction conversion. Figure 7 below shows a snapshot of the reactor in operation with areas of wetted and non-wetted traps.

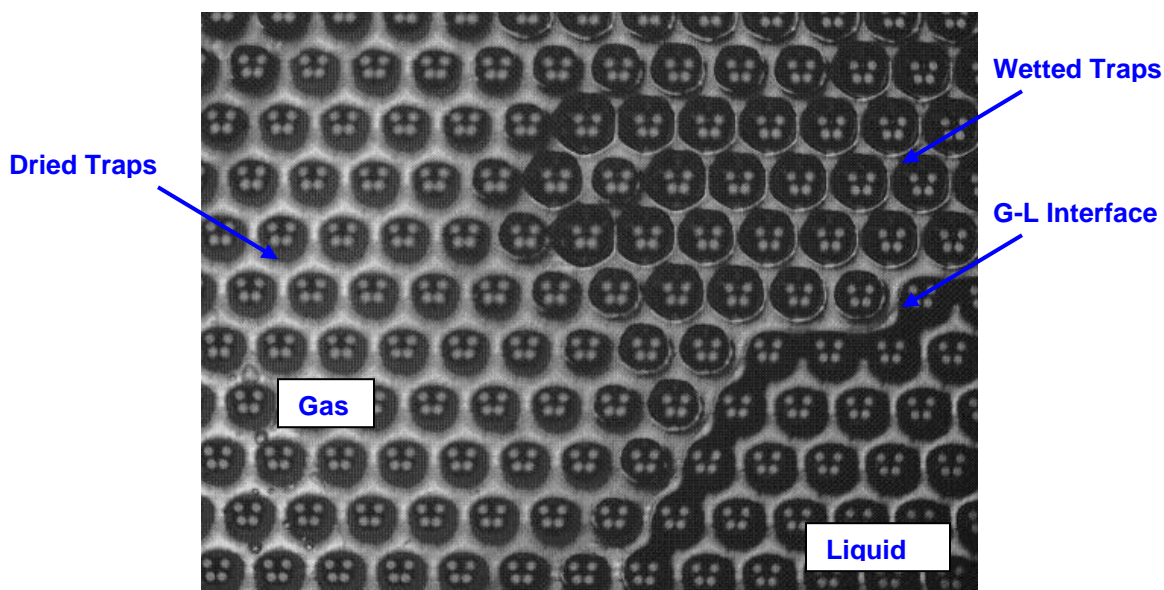


Figure 4- Reactor Photograph of Dried vs Wetted Traps

Conclusions and Future Work

After defining three gas-liquid flow regimes for the reactor, we began measuring conversion and selectivity at each point on the flow map. We found that the highest conversion falls within the transitional flow regime. The reaction is mass-transfer-controlled, as opposed to kinetically-controlled, and the turbulence induced by transitional flow provides the best gas-liquid and liquid-solid mass transfer. Experimental conversion is much higher than predicted by our kinetic model. The presence of wetted traps functioning as a network of small batch reactors is a possible cause for the discrepancy.

For future work, we should fill in conversion and selectivity for the remainder of the flow map. It is likely that $0.20\text{-}0.30\ \text{mL/min}$ will be the maximum feasible liquid flow rate if the reaction becomes limited by residence time. As liquid flow rate is increased, the transitional flow regime will shift to the right in Figure 5, so the range of gas flow rates should be expanded to accommodate several gas-dominated points. The flow map should also be duplicated at a higher hydrogen partial pressure to observe the effect of hydrogen liquid-phase concentration. Finally, we can explore the effect of wetted traps by revising the model to include some prediction of interfacial area and residence time in a series of tiny batch reactors.

Literature Cited

1. R.V. Chaudhari, M.G. Parande, P.A. Ramachandran, and P.H. Brahme; I. ChemE Symposium Series No. 87.
2. P.H. Brahme, H.G. Vadgaonkar, P.S. Ozarde, and M.G. Parande; J. Chem. Eng. Data 1982, 27, 461-462.
3. R.F. Guedes de Carvalho, A.M. Alves; AIChE Journal V. 45, Issue 12, Dec. 1999, 2495-2502.
4. A. Lawal, S. Tadepalli, R. Halder, H. Qiu, W.Y. Lee, R. Besser; AIChE Spring Meeting, Atlanta, GA, April 13, 2005.
5. E.H. Stitt; Chem. Eng. Journal 4025 (2002) 1-14.
6. J. Heiszwolf, M. Kreutzer, M. van den Eijnden, F. Kapteijn, J. Moulijn; Catalysis Today, 69 (2001) 51-55.
7. M. Kreutzer, F. Kapteijn, J. Moulijn, J. Heiszwolf; Chem. Eng. Science 60 (2005) 5895-5916.
8. M. Losey, R. Jackman, S. Firebaugh, M. Schmidt, K.F. Jensen; Journal of Microelectromechanical Systems, Vol. 11, No. 6, December 2002.
9. H.S. Fogler; *Elements of Chemical Reaction Engineering*, 4th Ed.; 2006
10. J.D. Seader and E.J. Henley; *Separation Process Principles*; 1998